



# Effect of radioactivity outside the field of view on image quality of dedicated breast positron emission tomography: preliminary phantom and clinical studies

Yoko Satoh<sup>1,2</sup> · Masamichi Imai<sup>1</sup> · Chihiro Ikegawa<sup>1</sup> · Kenji Hirata<sup>3</sup> · Norifumi Abo<sup>4</sup> · Mao Kusuzaki<sup>5</sup> · Noriko Oyama-Manabe<sup>6</sup> · Hiroshi Onishi<sup>2</sup>

Received: 5 July 2022 / Accepted: 20 September 2022 / Published online: 8 October 2022  
© The Author(s) under exclusive licence to The Japanese Society of Nuclear Medicine 2022

## Abstract

**Objective** Semi-quantitative positron emission tomography (PET) values, such as the maximum standardized uptake value ( $SUV_{max}$ ), are widely used to identify malignant lesions and evaluate the response to treatment. The image quality of ring-shaped dedicated breast positron emission tomography (dbPET) has been known to decrease the closer it is to the detector's edge. This study aimed to investigate the effect of radioactivity (RI) outside the detector field of view (FOV) on the image quality of the ring-shaped dbPET.

**Methods** A breast phantom containing the left myocardium, which was prepared using a 3D printer, filled with  $^{18}F$ -fluorodeoxyglucose (FDG) solution with various RI concentration ratios (RCRs) of myocardium to background and scanned with the edge of an apex positioned exactly in line with the edge of the FOV of the dbPET scanner. The phantom image quality was visually and quantitatively evaluated. Following the phantom study, left–right breast differences (the left breast uptake ratio to the right breast (LUR)) on clinical dbPET images of 74 women were quantitatively evaluated. The relationships between these parameters, clinical indices, and FDG uptake in the left myocardium on PET/computed tomography (CT) images were analyzed.

**Results** The phantom study showed that the higher the RCR of the myocardium and the closer it is to the top edge of the phantom, the higher is the pixel value of the dbPET images. In a clinical study, LUR was significantly correlated with myocardial  $SUV_{max}$  ( $r=0.96$ ,  $p<0.0001$ ) and metabolic myocardial volume ( $r=0.63$ ,  $p=0.001$ ) for whole-body PET/CT imaging. Although no significant correlations were found between LUR and age ( $r=0.05$ ,  $p=0.6865$ ), body mass index ( $r=0.03$ ,  $p=0.8178$ ), or distance between the left myocardial apex and chest wall ( $r=0.16$ ,  $p=0.1667$ ).

**Conclusions** FDG uptake in the myocardium affected dbPET images of the left breast, especially near the chest wall. Further, the effect of RI outside the FOV, such as in the myocardium, must be considered in the quantitative evaluation of breast cancer using dbPET.

**Keywords** Dedicated breast positron emission tomography ·  $^{18}F$ -fluorodeoxyglucose · Radioactivity outside the field-of-view (FOV) · Myocardial uptake · Phantom

✉ Yoko Satoh  
ysatoh@ypic.jp

<sup>1</sup> Yamanashi PET Imaging Clinic, Chuo City, Yamanashi Prefecture, Japan

<sup>2</sup> Department of Radiology, University of Yamanashi, Chuo City, Yamanashi Prefecture 409-3821, Japan

<sup>3</sup> Department of Diagnostic Imaging, Hokkaido University Graduate School of Medicine, Sapporo, Hokkaido, Japan

<sup>4</sup> Central Institute of Isotope Science, Hokkaido University, Sapporo, Hokkaido, Japan

<sup>5</sup> Research Institute for Electronic Science, Hokkaido University, Sapporo, Hokkaido, Japan

<sup>6</sup> Department of Radiology, Jichi Medical University Saitama Medical Center, Saitama, Japan

## Introduction

Breast cancer (BC) is the most common cancer and the second leading cause of cancer-related deaths among women with increasing incidences [1].  $^{18}\text{F}$ -fluorodeoxyglucose (FDG) positron emission tomography/computed tomography (PET/CT) has become one of the most useful tools for identifying distant metastases or secondary cancer, staging, and monitoring response to therapy [2, 3]. PET is more quantitative than other conventional diagnostic imaging modalities, and semiquantitative values of PET, such as  $\text{SUV}_{\text{max}}$ , are widely used to differentiate between benign and malignant tumors, predict prognosis, and determine the response to treatment.

In the recent years, dedicated breast PET (dbPET), which specializes in breast imaging, has been developed to provide better sensitivity and spatial resolution than whole-body PET [4, 5]. Ring-shaped high-resolution breast PET scanners have greater sensitivity and can improve spatial resolution by setting the detector close to the breast and reducing respiratory movement by scanning in the prone position. However, dbPET images have high levels of noise at the edge of the detector (the top of the detector, that is, the chest wall side) and lower image quality closer to the edge of the detector than in the center [6, 7]. This may be because the sensitivity of PET detectors decreases closer to the top and bottom edge of the detector compared to the center of the detector, and because of the effect of scattered radiation from FDG accumulated in the trunk, especially in the left myocardium, which is outside the field-of-view (FOV) of the top of the detector. In PET/CT, on the other hand, there is no radioactivity (RI) outside the transverse FOV. Although RI exists outside the longitudinal FOV, the image quality at the top and bottom edges of the FOV is improved by overlap acquisition. Because the geometry of organ-specific PET, such as dbPET significantly differs from that of PET/CT, the effect of RI outside the FOV must be determined separately. Therefore, this study aims to investigate the effect of RI outside the upper top of the detector FOV on the image quality of ring-shaped dbPET.

## Methods

This single-institution study was approved by the Institutional Review Board of the Kofu Neurosurgical Hospital and Yamanashi PET Imaging Clinic in accordance with the Declaration of Helsinki. Because of the retrospective study design and use of anonymized patient data, the requirement for informed consent was waived.

## Ring-shaped dbPET

The dbPET scanner (Elmammo, Shimadzu Corp., Kyoto, Japan) consists of 36 detector modules arranged in three contiguous rings, with a diameter of 195 mm, transaxial length of 156.5 mm, and depth-of-interaction measurement (DOI) capability [8]. The dbPET system uses a 3.4 ns coincidence time window, a random correction using singles count rates, and a 3 mm thick tungsten top shield for the end shield. Although undisclosed, a wide energy window is set up, from the first to the fourth layer of the DOI detector. The transaxial effective FOV was 185 mm. Each detector block consisted of a four-layered  $32 \times 32$  array of lutetium oxyorthosilicate crystals ( $1.44 \text{ mm} \times 1.44 \text{ mm} \times 18 \text{ mm}$  in size with a DOI layer 4.5 mm tall) coupled to a 64-channel position-sensitive photomultiplier tube via a light guide. Attenuation correction was calculated using a uniform attenuation map with object boundaries obtained from emission data [9]. Scatter correction was performed using the convolution–subtraction method with kernels obtained by background-tail fitting [10]. The characteristics and standard performance of this scanner have been previously reported in detail [11].

## Phantom design

A phantom that contained the left myocardial cavity in the background of a cylinder that corresponded to the mammary gland was custom-designed (Fig. 1). The size and shape of the left myocardial cavity and its position was designed based on chest CT measurements of 10 women (age range: 30–66 years; mean: 52 years) in the prone position with the breast naturally hanging. The myocardial cavity was prepared on a Form3® 3D Printer (Formlabs, USA) operating with low force stereolithography (LFS) technology. The build material (Photopolymer Resin) Clear Resin is a UV-curable plastic with a density of 1.15–1.20 g/mL (25 °C). The molded myocardial cavity was glued to a commercially available round acrylic sheet (thickness 5 mm) and acrylic pipe ( $\varnothing 100 \text{ mm}$ ) using light-curable adhesive. The phantom was placed so that the apex of the left myocardial cavity was immediately at the upper edge line of the detector, and then scanned for 20 min in list mode for each RI concentration ratios (RCR) of the myocardium.

## Data acquisition and image reconstruction

The background RI concentrations at the start of data acquisition were set to 2.1 kBq/mL for dbPET scan. The myocardial cavity was filled with an  $^{18}\text{F}$ -FDG solution with RCRs to the background of 1, 4, 8, and 16. RCRs were determined based on the findings of the previous studies [12, 13].

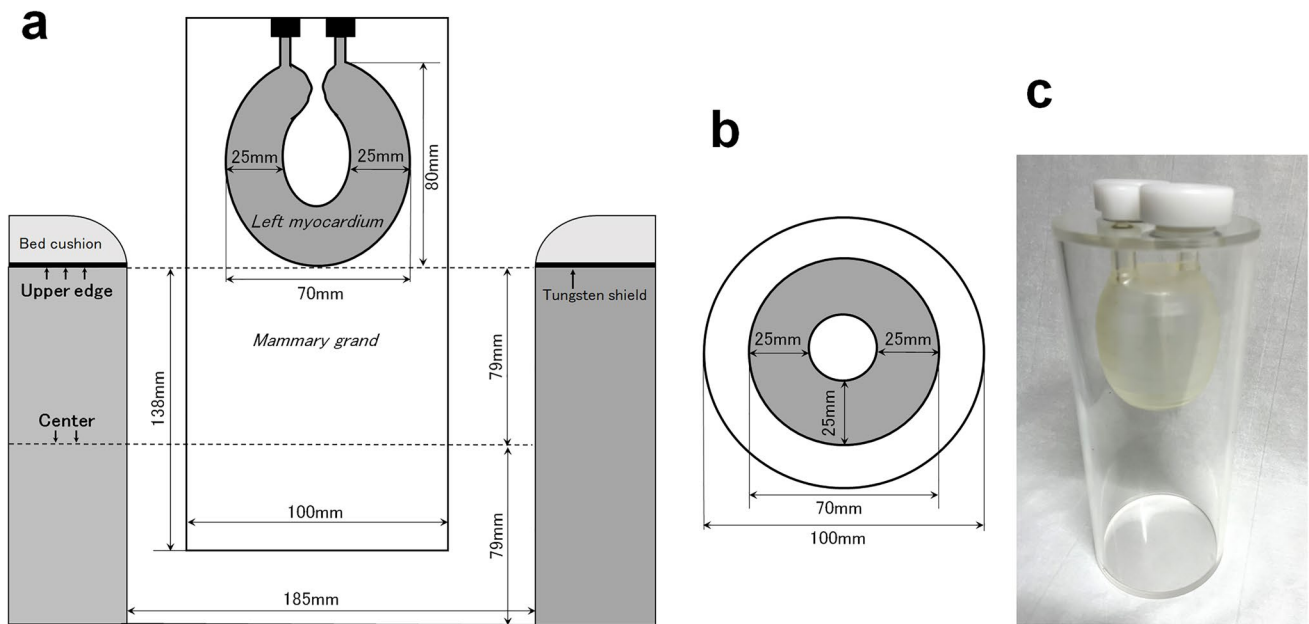


**Fig. 1** Dimensions of a custom-made breast phantom with left myocardium in place. Lateral view showing the relationship between the dbPET detector and the breast phantom (**a**); cross-sectional view of

the breast phantom (**b**); and photograph of the phantom (**c**). The values in the figure represent the length (mm)

The dbPET images were reconstructed using a three-dimensional list mode dynamic row-action maximum-likelihood algorithm with one iteration and 128 subsets, a relaxation control parameter of  $\beta=20$ , a matrix size in the axial view of  $236 \times 200 \times 236$  with a post-reconstruction smoothing Gaussian filter (1.17 mm full width at half-maximum (FWHM)), and scatter correction. The reconstructed voxel size of the dbPET images was  $0.78 \text{ mm} \times 0.78 \text{ mm} \times 0.78 \text{ mm}$ . These conditions were determined based on those used in the previous study with dbPET [14].

### Analyses of phantom image quality

All quantitative analyses of phantom and clinical PET images used in this study were performed using an in-house-modified Metavol [15]. Standardized uptake values (SUVs), as a semi-quantitative assessment of pixel values, were extracted using this software.

The SUV of a given was calculated using the following formula:

$$\begin{aligned} \text{SUV} &= \frac{\text{RI concentration (Bq/ml)}}{\text{decay - corrected quantity of RI (Bq)}} \\ &\quad \times \text{phantom volume (ml)} \\ &= \frac{\text{Tumor activity concentration (Bq/ml)}}{\text{Injected dose (Bq)}} \\ &\quad \times \text{body weight (g)}. \end{aligned}$$

For the quantitative analysis of phantom images, 14 spherical volumes of interest (VOIs) with a diameter of 16 mm were placed on three transverse slices (center of the detector, and 2 cm and 1 cm from the upper edge of the detector, Fig. 2). The mean SUVs ( $\text{SUV}_{\text{mean}}$ ) are the average values within the VOI. The coefficient of variation ( $\text{CV}_{\text{BG}}$ )

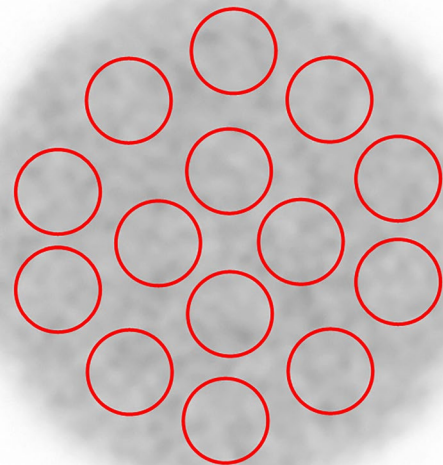


**Fig. 2** Position of the VOI for the measurement of dbPET phantom images. Fourteen 16 mm diameter VOIs were placed on a dbPET image of the phantom for the measurement of  $\text{CV}_{\text{BG}}$  and  $\text{SD}_{\Delta\text{SUV}_{\text{mean}}}$

and uniformity ( $SD_{\Delta SUV_{mean}}$ ) of the background were calculated using data from all VOI measurements as follows:

$$CV_{BG} = \text{mean of} \left[ \frac{SD_{BG,16mm}}{C_{BG,16mm}} \times 100 \right] (\%),$$

$$SD_{\Delta SUV_{mean}} = \sqrt{\frac{1}{n-1} \sum_{i=1}^n (\Delta SUV_{mean,i})^2},$$

where  $SD_{BG,16mm}$  is the standard deviation of the background VOI values for a 16-mm-diameter sphere,  $C_{BG,16mm}$  is the average of the background VOI values for a 16-mm-diameter sphere, and  $\Delta SUV_{mean}$  is the relative error of each background VOI value for a 16-mm-diameter sphere. These physical assessments were performed according to the previous reports [7, 14].

### Analysis of human images

Subjects of PET scan fasted for at least 6 h before administration of  $^{18}\text{F}$ -FDG (3 MBq/kg). Chest PET/CT scanning was performed prior to dbPET 60 min after the injection using a whole-body PET/CT scanner (Biograph Horizon; Siemens Medical Solutions, Erlangen, Germany). Chest PET/CT was performed in the prone position using a device that allowed the breast to hang naturally. PET/CT images were reconstructed using the ordered subset expectation maximization method and the time-of-flight algorithm with four iterations and ten subsets. The CT data were resized from a  $512 \times 512$  matrix to a  $180 \times 180$  matrix to match the PET data and construct CT-based transmission maps for attenuation correction of the PET data with a post-reconstruction smoothing Gaussian filter (5 mm FWHM). After the PET/CT scan, approximately 90 min after FDG injection, dbPET scanning was performed also in the prone position. The breasts were scanned with dbPET for 7 min each, first on the right side and then on the left side. Clinical dbPET images were reconstructed under the same conditions as the phantom images.

Between January 2019 and December 2020, 80 women underwent chest PET/CT and dbPET for BC screening at our institution. Women who were identified with abnormal uptakes ("focal", "mass", or "non-mass" uptake based on the previous report [16]) on the dbPET images by a diagnostic radiologist of breast imaging and nuclear medicine physician were excluded. Consequently, a total 74 women were included in this study.

For quantitative evaluation, nine VOIs with a diameter of 10 mm were placed 20 mm from the edge of the FOV, referring to the transverse and sagittal images of dbPET including the nipple (Fig. 3). Five VOIs were equally placed on these images including the nipple, avoiding the skin and

without consideration of structures (fat, mammary glands, etc.) within the VOIs. One VOI located at the intersection of the transverse and sagittal images was common in both sections, for a total of nine VOIs were placed for one breast. The left breast uptake ratio to the right breast (LUR) was calculated using the following formula:

$$LUR = \frac{\overline{SUV_{mean,Lt}} - \overline{SUV_{mean,Rt}}}{\overline{SUV_{mean,Rt}}} \times 100\%$$

where  $\overline{SUV_{mean,Lt}}$  and  $\overline{SUV_{mean,Rt}}$  are the average  $SUV_{mean}$  of the nine VOIs for the left and right breasts, respectively.

The average of the values measured once by a nuclear medicine physician (YS) and a radiological technologist (MI) were used in the analysis. In addition, the shortest distance between the apex of the left myocardium and the chest wall (Dist), the  $SUV_{max}$  of the left myocardium ( $SUV_{max,myo}$ ), and volume with an SUV of 2.5 or more (metabolic myocardial volume (MMV)  $\text{cm}^3$ ) were measured on chest PET/CT images. Although "Dist" should be measured from the FDG accumulation on PET images, in cases where the FDG accumulation in the myocardium was low, the boundary of the myocardium on PET images was not clear, and decrease in the reproducibility of the measurement was a concern. Therefore, "Dist" was measured from CT, which has a clearer boundary than PET image.

### Statistical analysis

Regression analyses between LUR and the clinical indicators or PET-derived parameters were performed using Pearson's correlation coefficient. The intraclass correlation coefficient (ICC), based on the two-way random effects model, was used to assess the agreement of LUR measurements

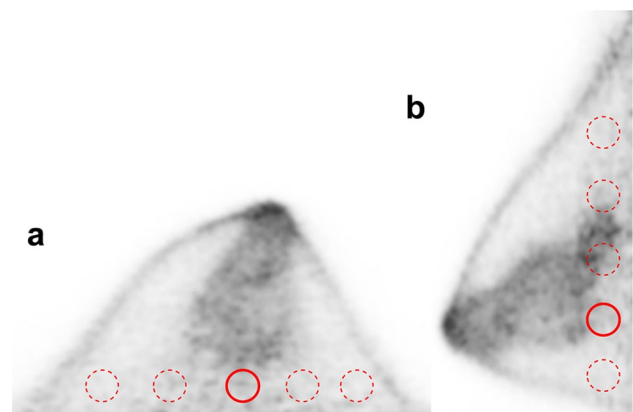


**Fig. 3** Position of the VOI for the measurement of clinical dbPET images. Nine spherical VOIs (bold circles represent the same VOI) were placed to calculate the LUR. Transaxial (a) and sagittal (b) images of dbPET

between the two readers. Statistical significance was defined as  $p < 0.05$ . JMP<sup>®</sup>16 (SAS Institute Inc., Cary, NC, USA) was used for all the analyses.

## Results

### Phantom studies

Transverse images of the dbPET phantoms with different myocardial RCRs are shown in Fig. 4. The phantom images showed that the higher the RCR of the myocardium, the higher was the pixel value of the FOV upper edges (Fig. 4a, b). In addition, even in the image at the center of the detector, higher RCRs could result in higher pixel values near the outer edge of the phantom. An unexpected behavior was observed in the center of the detector (Fig. 4c), where pixel values were higher at the lateral edges for RCRs 1, 8, and 16, whereas they were uniform for RCR of 4.

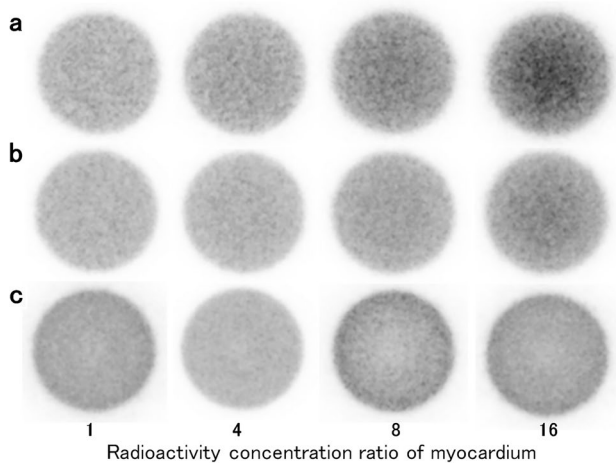


**Fig. 4** Transverse phantom images with different myocardial RCRs and different positions. Transverse phantom images at 1 cm (a) and 2 cm (b) from the upper edge and at the center of the dbPET detector (c). Phantom images were displayed with an SUV range of 0–4

In the quantitative evaluation of phantom images,  $SUV_{mean}$  and  $CV_{BG}$  were higher at the edge of the detector as myocardial accumulation was higher, whereas they did not vary with myocardial accumulation at the center of the detector. Furthermore, when myocardial accumulation was high,  $SD_{\Delta SUV_{mean}}$  was also higher and closer to the detector edge, whereas it did not vary with location within the detector when myocardial accumulation was low (Fig. 5).

### Clinical studies

A total of 74 women (age range 25–84 years; mean age 53 years) were evaluated. Table 1 shows the mean and range of their body mass index (BMI), Dist,  $SUV_{max,myo}$ , and MMV. The ICC for LUR was moderate (0.57). There was no significant correlation between the LUR and age (Fig. 6a,  $p = 0.6865$ ), BMI (Fig. 6b,  $p = 0.8178$ ), or Dist (Fig. 6c,  $p = 0.1667$ ). In contrast, the median (range) LUR was 5.98% (from -50.15 to 54.93), which was significantly correlated with  $SUV_{max,myo}$  (Fig. 6d,  $r = 0.96$  and  $p < 0.0001$ ) and MMV (Fig. 6e,  $r = 0.63$  and  $p = 0.001$ ). Figure 7 shows representative PET images of normal breasts with high or low FDG uptake in the myocardium. For a woman with myocardium with higher FDG uptake on the chest PET/CT image (Fig. 7a, b), noise increased near the chest wall on the dbPET image (Fig. 7c), which was located near the upper edge of the detector.

**Table 1** Characteristics of 74 participants

	Mean [range]
Age (years)	53 [25–84]
BMI	22.64 [15.1–36.05]
Dist (mm)	17.87 [7–43]
$SUV_{max,myo}$	5.54 [1.75–17.66]
MMV (cm <sup>3</sup> )	62.36 [0–226.24]

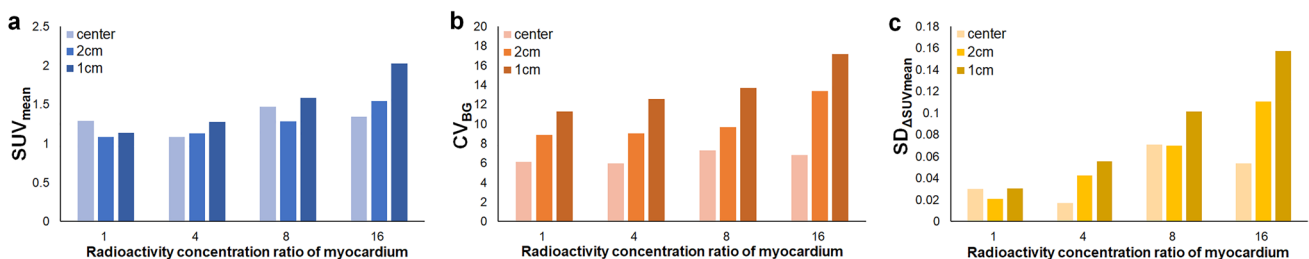


**Fig. 5** Quantitative evaluation of phantom images.  $SUV_{mean}$  (a), coefficient of variation of the background (b), and  $SD_{\Delta SUV_{mean}}$  (c) with different RCRs and the position in the detector

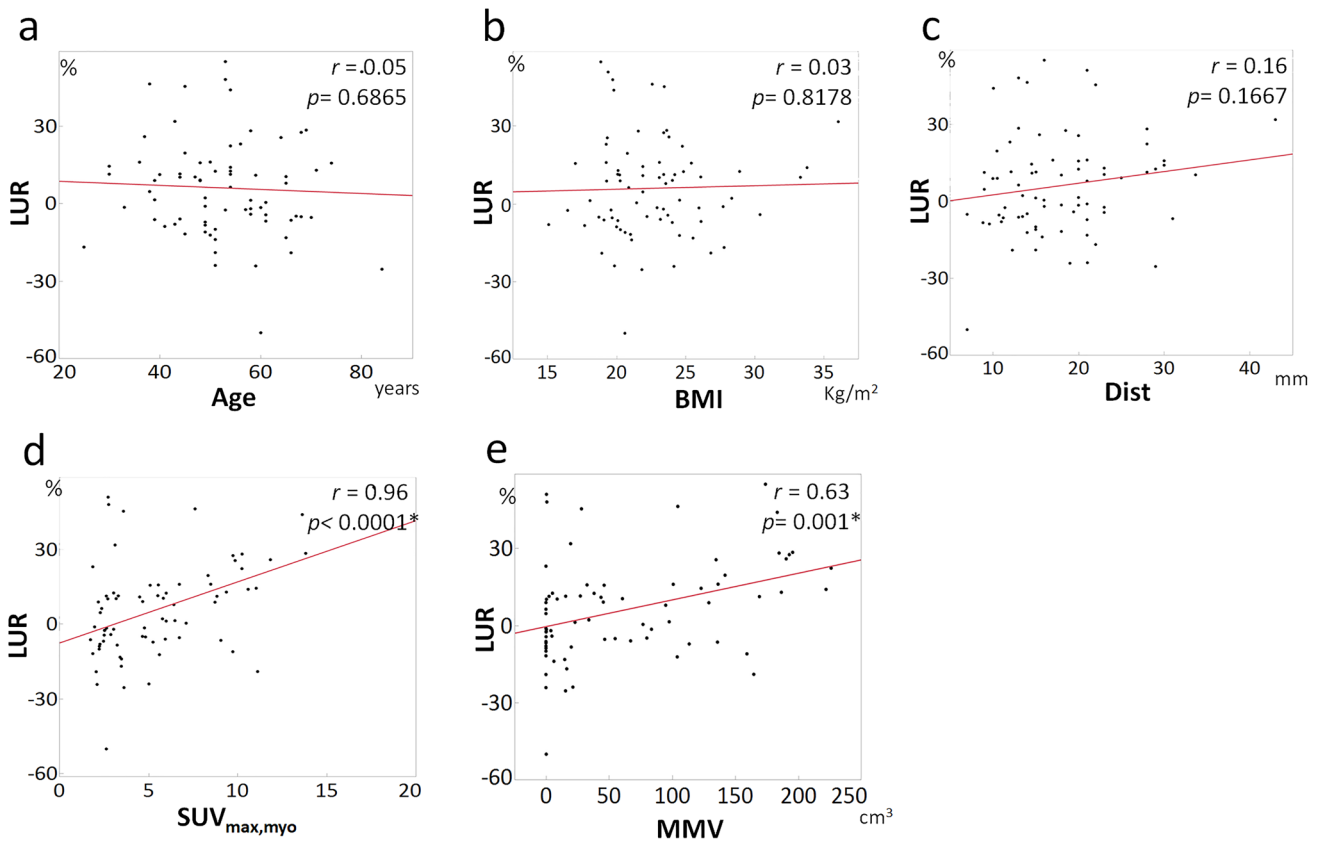
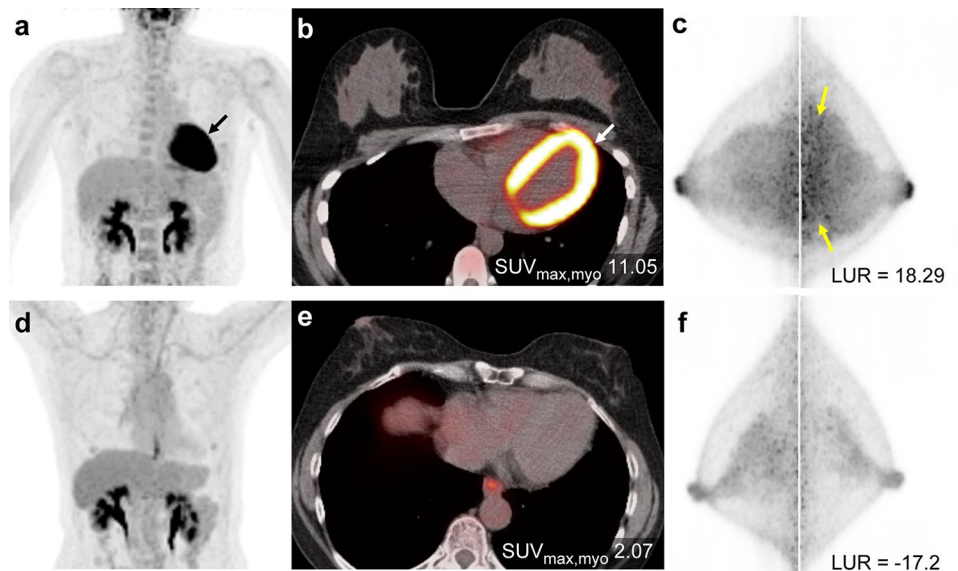


**Fig. 6** Relationship between LUR and clinical or image derived parameters. Regression analysis results for LUR and age (a), BMI (b), Dist (c),  $SUV_{max,myo}$  (d), and MMV (e)

**Fig. 7**  $^{18}F$ -FDG PET/CT and dbPET images scanned in the prone position. Maximum intensity projection (MIP) (a, d) and transaxial fusion images of PET/CT (b, e), and MIP of dbPET (c, f). For a woman in her 30 s (a–c), laterality was observed in dbPET images (yellow arrow), which is due to the effect of the high radioactivity in the myocardium (black and white arrows), as shown in the upper row. In contrast, for women in her 60 s, FDG uptake into the myocardium was low, and dbPET images did not affect the FDG uptake of the myocardium, as shown in the lower row.



## Discussion

In this study, the image quality of a breast phantom with varying RCR of the myocardium close outside the upper edge of the detector was first evaluated at different vertical positions in the detector. The results showed that the SUVs were overestimated and became more heterogeneous closer to the edge of the cylindrical detector, and the degradation was worse with a higher myocardial RCR. These results were consistent with the previous reports that found that dbPET image quality decreases at the edge of the detector [6, 7]. Furthermore, an unexpected behavior was observed at the center of the detector (Fig. 4c), where the pixel values were not uniform and higher at the lateral edges of the FOV when the RCR was 1, 8, and 16. For dbPET attenuation correction, an attenuation map obtained by detecting the object boundary from dbPET emission data and assuming that its interior has a uniform fat absorption value is used. For the first time, this unexpected behavior was shown, since previously reported phantom studies did not consider RI outside FOV [4, 7, 11, 14]. Our results indicated that the RI outside the FOV prevented to obtain accurate attenuation correction maps, which may have been one of the reasons for the degraded dbPET image quality. Recently, it has been reported that a new organ specific—proximity type of PET system implements an another attenuation correction method based on a new maximum-likelihood attenuation correction factor [17]. It has been shown in the previous study that the new attenuation correction method can be used to obtain an attenuation map of the head, including bone, derived from PET emission data. The next and subsequent phantom-based studies with RIs outside the FOV at various different RI concentrations and locations should clarify this behavior.

Commercially available dbPET system for clinical use have sensitivity and scatter correction implemented [4, 13, 14]. However, our clinical studies suggest that FDG accumulation in the myocardium would affect the image quality of dbPET images, mainly in the left breast, especially on the chest wall side. This means that the correction methods currently implemented in dbPET scanners are not sufficient to correct for the effects of RI outside the FOV. However, given that the degree of myocardial accumulation varies from day to day in the same patient and that the dbPET image data does not contain information on the amount and location of RI outside the FOV, it would be difficult to correct for the true value of FDG accumulation in the breast using dbPET scans alone.

Based on these results, the use of indicators of myocardial FDG accumulation obtained from whole-body or chest PET/CT images acquired prior to dbPET scans may be considered for the correction of dbPET images. It has been reported that PET/CT scans in the prone position are more useful for detecting small lesions in the breast than those in the supine position [18, 19]. However, it is not widely used in daily practice because scanning the whole-body from the head to the lower leg in the prone position is painful for the patient; therefore, the patient is currently scanned in the supine position in routine practice. Nevertheless, the positional relationship between the breast and myocardium in the prone PET/CT scan used in this study was almost the same as that in the dbPET scan, and PET/CT can provide anatomical positional information that cannot be obtained from dbPET. Therefore, an index based on PET/CT images may be used in the future to correct dbPET images. If this scanning method is shown to be useful in improving the quantitative performance of dbPET images in the future, it should be possible to prepare a routine protocol for BC patients and study a larger number of cases.

The usefulness of SUVs, such as their association with the grade and prognosis of BC, has been shown in many previous studies [20, 21]. Because  $SUV_{max}$  is the maximum pixel value contained in the VOI, the measurement is highly reproducible and easy to use. dbPET and whole-body PET/CT have also been reported to be useful in differentiating between subtypes and benign/malignant tumors [5, 16]. Therefore, further studies are needed to define a correction method for the SUV of dbPET images from whole-body PET/CT data using a phantom containing hot spheres. In addition, those spheres should be variable in order to consider the variation in quantification due to their position in the detector.

Our study has several limitations. First, unlike phantom studies in general PET studies, our phantom did not contain a sphere corresponding to the intra-breast lesion. This was done to avoid the effect of FDG in the sphere on the surrounding image quality for evaluating the fine image quality at the edges of the high-sensitivity detector. However, a phantom containing spheres corresponding to breast lesions may be more clinically relevant. The results of adequate correction method of SUV on dbPET will be shown in a future study using a phantom containing hot spheres. Second, the design of this clinical study was retrospective, and the patient cohort was small. If PET/CT scan in the prone position is shown to be useful for improving the quantitative quality of dbPET images, it could be widely adopted as a routine protocol for BC patients, allowing future studies with large amounts of patient data.

## Conclusions

In conclusion, FDG uptake in the myocardium affected dbPET images of the left breast, especially near the chest wall. It is necessary to consider the effect of RI outside the FOV, such as in the myocardium, in the quantitative evaluation of BC with dbPET.

**Acknowledgements** We are thankful to Mr. Tetsuro Mizuta and Mr. Yuichi Inaoka from Shimadzu for technical support of dbPET scanner. We would like to thank Editage (www.editage.jp) for English language editing. No potential conflicts of interest were disclosed.

**Funding** The phantom used in this study was prepared with the support of the Japan Society for the Promotion of Science (JSPS) Grant-in-Aid for Scientific Research No. JP20K08042.

## Declarations

**Conflict of interest** The authors declare that they have no competing interests.

**Ethical approval** This study has been approved by the review board of the Kofu Neurosurgical Hospital to which our institution belongs (approval date: June 3, 2021).

**Consent to participate** Due to the retrospective study design and the use of anonymized patient data, the need for consent to participate was waived by the ethics committee that approved our study. All procedures performed in studies involving human participants were in accordance with the ethical standards of the institutional and/or national research committee and with the 1964 Helsinki declaration and its later amendments or comparable ethical standards.

## References

1. Siegel RL, Miller KD, Jemal A. Cancer statistics, 2020. *CA Cancer J Clin.* 2020;70:7–30. <https://doi.org/10.3322/caac.21590>.
2. Groheux D, Cochet A, Humbert O, Alberini JL, Hindié E, Mankoff D. <sup>18</sup>F-FDG PET/CT for staging and restaging of breast cancer. *J Nucl Med.* 2016;57(Suppl 1):17S-26S. <https://doi.org/10.2967/jnumed.115.157859>.
3. Satoh Y, Nambu A, Ichikawa T, Onishi H. Whole-body total lesion glycolysis measured on fluorodeoxyglucose positron emission tomography/computed tomography as a prognostic variable in metastatic breast cancer. *BMC Cancer.* 2014;14:525. <https://doi.org/10.1186/1471-2407-14-525>.
4. Satoh Y, Motosugi U, Imai M, Onishi H. Comparison of dedicated breast positron emission tomography and whole-body positron emission tomography/computed tomography images: a common phantom study. *Ann Nucl Med.* 2020;34:119–27. <https://doi.org/10.1007/s12149-019-01422-0>.
5. Sueoka S, Sasada S, Masumoto N, Emi A, Kadoya T, Okada M. Performance of dedicated breast positron emission tomography in the detection of small and low-grade breast cancer. *Breast Cancer Res Treat.* 2021;187:125–33. <https://doi.org/10.1007/s10549-020-06088-1>.
6. Minoura N, Teramoto A, Ito A, Yamamuro O, Nishio M, Saito K, et al. A complementary scheme for automated detection of high-uptake regions on dedicated breast PET and whole-body PET/CT. *Radiol Phys Technol.* 2019;12(3):260–7. <https://doi.org/10.1007/s12194-019-00516-8>.
7. Satoh Y, Motosugi U, Imai M, Omiya Y, Onishi H. Evaluation of image quality at the detector's edge of dedicated breast positron emission tomography. *EJNMMI Phys.* 2021;8:5. <https://doi.org/10.1186/s40658-020-00351-6>.
8. Tsuda T, Murayama H, Kitamura K, Yamaya T, Yoshida E, Omura T, et al. A four-Layer depth of interaction detector block for small animal PET. *IEEE Trans Nucl Sci.* 2004;51:2537–42. <https://doi.org/10.1109/TNS.2004.835739>.
9. Yamakawa Y, Kitamura K. Attenuation correction using level set method for application specific PET scanners. *IEEE Nucl Sci Symp Med Imaging Conf Rec.* 2011;p. 3130–2.
10. Bailey DL, Meikle SR. A convolution-subtraction scatter correction method for 3D PET. *Phys Med Biol.* 1994;39:411–24. <https://doi.org/10.1088/0031-9155/39/3/009>.
11. Miyake KK, Matsumoto K, Inoue M, Nakamoto Y, Kanao S, Oishi T, et al. Performance evaluation of a new dedicated breast PET scanner using nema NU4-2008 standards. *J Nucl Med.* 2014;55:1198–203. <https://doi.org/10.2967/jnumed.113.131565>.
12. Heusch P, Buchbender C, Beiderwellen K, Nensa F, Hartung-Knemeyer V, Lauenstein TC, et al. Standardized uptake values for [<sup>18</sup>F] FDG in normal organ tissues: comparison of whole-body PET/CT and PET/MRI. *Eur J Radiol.* 2013;82:870–6. <https://doi.org/10.1016/j.ejrad.2013.01.008>.
13. Sprinz C, Zanon M, Altmayer S, Watte G, Irion K, Marchiori E, et al. Effects of blood glucose level on <sup>18</sup>F fluorodeoxyglucose (<sup>18</sup>F-FDG) uptake for PET/CT in normal organs: an analysis on 5623 patients. *Sci Rep.* 2018;8:2126. <https://doi.org/10.1038/s41598-018-20529-4>.
14. Satoh Y, Imai M, Hirata K, Asakawa Y, Ikegawa C, Onishi H. Optimal relaxation parameters of dynamic row-action maximum likelihood algorithm and post-smoothing filter for image reconstruction of dedicated breast PET. *Ann Nucl Med.* 2021;35:608–16. <https://doi.org/10.1007/s12149-021-01604-9>.
15. Hirata K, Kobayashi K, Wong KP, Manabe O, Surmak A, Tamaki N, et al. A semi-automated technique determining the liver standardized uptake value reference for tumor delineation in FDG PET-CT. *PLoS ONE.* 2014;9: e105682. <https://doi.org/10.1371/journal.pone.0105682>.
16. Satoh Y, Motosugi U, Omiya Y, Onishi H. Unexpected abnormal uptake in the breasts at dedicated breast PET: incidentally detected small cancers or nonmalignant features? *AJR Am J Roentgenol.* 2019;212:443–9. <https://doi.org/10.2214/AJR.18.20066>.
17. Mizuta T, Kobayashi T, Yamakawa Y, Hanaoka K, Watanabe S, Morimoto-Ishikawa D, et al. Initial evaluation of a new maximum-likelihood attenuation correction factor-based attenuation correction for time-of-flight brain PET. *Ann Nucl Med.* 2022;36:420–6. <https://doi.org/10.1007/s12149-022-01721-z>.
18. Canevari C, Gallivanone F, Zuber V, Marassi A, Losio C, Gianolli L, et al. Prone <sup>18</sup>F-FDG PET/CT changes diagnostic and surgical intervention in a breast cancer patient: some considerations about PET/CT imaging acquisition protocol. *Clin Imaging.* 2015;39:506–9. <https://doi.org/10.1016/j.clinimag.2014.11.005>.
19. Teixeira SC, Koolen BB, Vogel WV, Wesseling J, Stokkel MP, Vrancken Peeters MJ, et al. Additional prone <sup>18</sup>F-FDG PET/CT acquisition to improve the visualization of the primary tumor and regional lymph node metastases in stage II/III breast cancer. *Clin Nucl Med.* 2016;41:e181–6. <https://doi.org/10.1097/RLU.0000000000001101>.
20. Akdeniz N, Kömek H, Küçüköner M, Kaplan MA, Uraçkı Z, Oruç Z, et al. The role of basal <sup>18</sup>F-FDG PET/CT maximum standard uptake value and maximum standard uptake change in predicting pathological response in breast cancer patients receiving



- neoadjuvant chemotherapy. *Nucl Med Commun.* 2021;42:315–24. <https://doi.org/10.1097/MNM.0000000000001332>.
21. Öner H, Canaz F, Diğer M, Işıksoy S, Sivriköz İA, Entok E, et al. Which of the fluorine-18 fluorodeoxyglucose positron emission tomography/computerized tomography parameters are better associated with prognostic factors in breast cancer? *Medicine.* 2019;98: e15925. <https://doi.org/10.1097/MD.00000000000015925>.

**Publisher's Note** Springer Nature remains neutral with regard to jurisdictional claims in published maps and institutional affiliations.

Springer Nature or its licensor holds exclusive rights to this article under a publishing agreement with the author(s) or other rightsholder(s); author self-archiving of the accepted manuscript version of this article is solely governed by the terms of such publishing agreement and applicable law.